Chapter

Theoretical Prediction and Optimization Approach to Triboelectric Nanogenerator

He Zhang and Liwei Quan

Abstract

Triboelectric nanogenerator (TENG) is a new type of electrostatic generator based on the principle of Maxwell displacement current. It could be designed as a device for either smart sensing or energy harvesting via converting mechanical energy into electric power efficiently. To predict its output characteristic, investigate its working mechanism, and enhance its working performance, the theoretical analysis and optimization work in either experimental or theoretical means are of great significance. In this chapter, we plan to introduce the progress of theoretical analysis and optimization approach to TENG with four different modes. Three parts of work will be introduced in the manuscript: (1) the theoretical prediction approach for electric output performance of TENG device, (2) the optimization strategies for TENG device based on figure of merits, and (3) the scaling laws between the normalized electric outputs and multiple physical properties of the TENG device.

Keywords: triboelectric nanogenerator, theoretical analysis, scaling law, optimization strategy

1. Introduction

Triboelectric nanogenerator (TENG) [1, 2] is a revolutionary mechanical energy harvesting technology based on triboelectrification and induction effects of two materials with opposite electric polarities. This device contains two dissimilar dielectric films facing with each other, and there are electrodes deposited on the top and the bottom surfaces of the two films. The working mechanism of TENG is based on triboelectric effect and principle of displacement current. TENG may utilize the surface electrostatic charges produced in physical contact-separation process of the two insulators to generate electric power. By separating the tribo-pair with contact-induced triboelectric charges, a potential drop will be generated which forces the electrons to flow between the two electrodes. Compared with other renewable energy technologies including solar cells [3], biofuels [4], tide generator [5], etc., TENGs are less restricted by environmental or climatic conditions. In applications of mechanical energy harvesting, TENGs have much higher power output and energy conversion efficiency than those of electromagnetic [6] and piezoelectric energy harvesters [7–11]. Besides, TENGs can be made from low-cost materials by easy manufacture processes because of its simple device structures and

configurations. These advantages make this new technology a better choice as power source for devices and microsystems [1, 2].

TENG has four basic operational modes with different structures: contact-separation mode, sliding mode, single-electrode mode, and freestanding mode. As **Figure 1** shows, these different modes are designed to meet the needs in different fields of applications. Based on these four modes, various TENG devices have been developed for different applications. Using these four modes and their combinations, a range of TENG devices have been invented for energy harvesting like wind and water, structure vibration and biomechanical motion energy harvesters, and self-powered smart sensing like vector sensor, tactile sensor, vibration detection, human physical signal detection, etc. [12–16].

With the progress of materials, structure design, and theories in fundamental mechanisms, the output performance of TENG is improved vigorously. Since its invention, the output power density of TENGs increases from initially a few $\mu W/m^2$ and mW/m^2 to tens of W/m^2. In recent works, a TENG with power density up to 500 W/m^2 and energy conversion efficiency more than 70% has been achieved, which is adequate to power most microelectronic devices and systems [2]. It is the optimization that makes the performance of the device greatly improved.

To further improve the output performance of the device, optimization design is of great importance and has already attracted attentions. In early works, the development of a new type of TENG devices or optimization of TENG design is typically realized through trial-and-error process experimentally, which is of high cost and time-consuming. Compared with experimental means, theoretical analysis is useful and more powerful in understanding the working mechanism of the device and could offer better optimization strategy for device structural design, material selection, and operation conditions. It is more convenient to realize the optimization of TENG with theoretical method rather than in experimental means. Based on the basic working mechanism of TENGs, the theoretical models for TENG have been established, a series of parameter analysis works have been carried out, and the relationship between the parameters and the output performance is obtained [17–21]. In addition, to establish a standard for evaluating different architectures

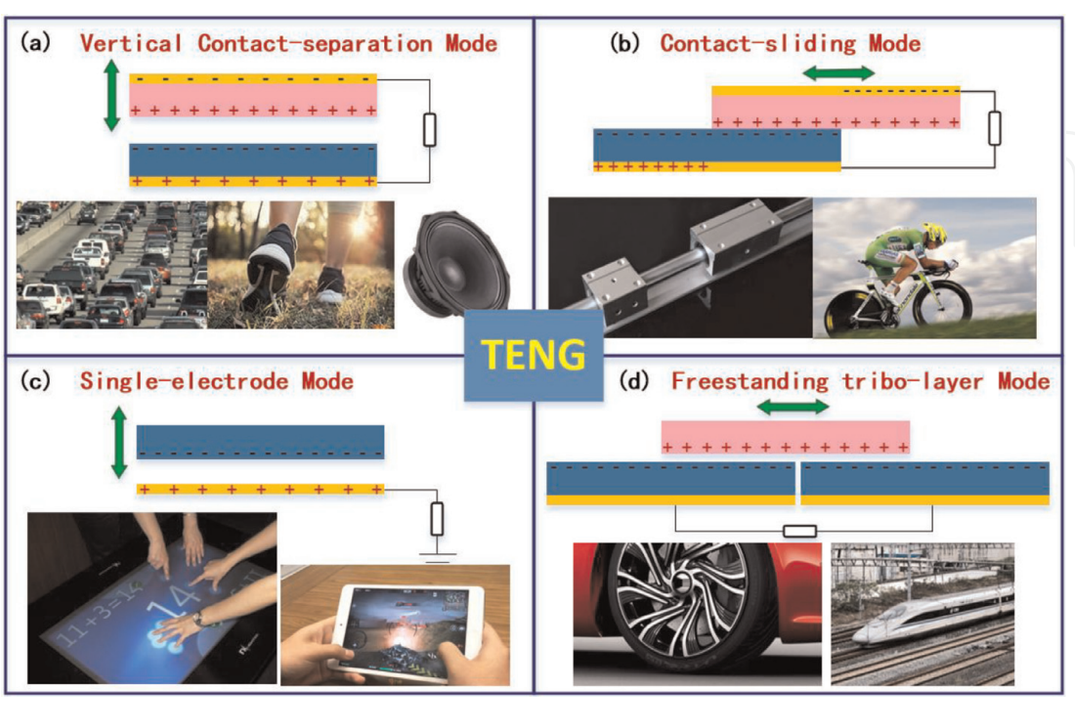

Figure 1.
Four fundamental modes of triboelectric nanogenerator [1].

of a TENG device, the device figure of merits of TENG is proposed and used to determine the maximum output power density of a TENG [22–24].

Although various theoretical models have been established for TENG, most of them are based on single-parameter analysis which focuses on investigating the effect of single variable on device performance with others fixed. For instance, in optimization of the thickness of dielectric materials, we may obtain its effect with other parameters fixed. The same procedure is required in repetition for other working conditions with different sets of fixed parameters. Yet the optimized structures and conditions may not be the best as many parameters are correlated.

To address this problem, Zhang proposed a set of formulations for normalized electrical outputs of the device in dimensionless forms [25, 26]. The expressions for these normalized outputs rely on two compound parameters composed of device dimensions (sizes, dielectric layer thickness), electrical properties of the electrode and dielectric materials, loading conditions (loading force, frequency, and motor process), and the circuit conditions (open/short circuit and load resistance). With these expressions, a multiparameter analysis method for theoretical approach for optimization of TENG has been derived. This method makes it possible to realize the optimization of the device by tuning different physical parameters simultaneously, which may reveal the real situation of the TENG that its output performance is influenced simultaneously and coherently by a number of factors.

In this chapter, the theoretical approaches of V-Q-x relationship for different TENGs are presented. Along with these relationships, the output performance of TENG and the optimization method with material and device figure of merits for TENG are discussed. Lastly, the multiparameter analysis method and the optimization strategy for TENG are presented.

2. The theoretical prediction and optimization strategies for TENG

In this section, the theoretical prediction for output performance and optimization strategies for design of TENG are discussed from three different aspects: the theoretical prediction approach for V-Q-x relationship of different modes of TENGs is presented firstly, followed by the principle of material and structure figure of merit for different modes of TENG and corresponding optimization strategies, and, lastly, the scaling laws between the normalized electric output of TENG and multiple physical properties are derived, with which the optimization strategies for TENG are provided.

2.1 The V-Q-x relationship of TENG

The four basic modes of TENG are of similar structure with two layers of different materials (dielectric-dielectric or dielectric-electrode), which are usually called tribo-pair. When the tribo-pair comes into contact, some charges move from one material to another to equalize their electrochemical potential due to triboelectric effect. When forced to separate, some of the surface charges tend to keep the original state, while the others tend to give electrons away, possibly producing triboelectric charges on the surfaces. The presence of triboelectric charges on dielectric surfaces can be a force for driving electrons in the electrode to flow in order to balance the electric potential drop created.

As **Figure 1** shows, there are two different motion patterns including contact-separation and sliding in these four modes of TENG. For the contact-separation mode and single-electrode mode TENG, the tribo-pair moves vertically and creates an air gap in between, while for the contact-sliding mode and freestanding

tribo-layer mode, the tribo-pair moves laterally. For these two different kinds of motion process, the theoretical models are quite different, which will be discussed in Sections 2.1.1 and 2.1.2, respectively.

2.1.1 Contact-separation mode TENG

According to the materials used and device structures, the contact-separation mode TENGs fall into two categories: dielectric-to-dielectric contact and conductor-to-dielectric contact structures (**Figure 2**). Based on Gauss's law, we may consider this kind of TENG as a series of flat plate capacitors; the relationship between electric field E in the tribo-pair and the total charge density ρ is $\nabla \cdot E = \rho/\varepsilon_0$. When the charged surfaces move, according to Maxwell's equations, the electric displacement field is defined as $D = \varepsilon_0 E + P$; therefore, the current density is $J_D = \varepsilon_0 \frac{\partial E}{\partial t} + \frac{\partial P}{\partial t}$. Thus, we can get the V-Q-x relationship of TENG [18].

The thicknesses of the dielectric plates in tribo-pair are assumed to be d_1 and d_2 with the relative dielectric constants ε_{r1} and ε_{r2}, respectively. According to the Gauss theorem, the electric field strengths of each layer in the dielectric-to-dielectric mode TENG are $E_1 = -Q/S\varepsilon_0\varepsilon_{r1}$ for dielectric plate 1, $E_2 = -Q/S\varepsilon_0\varepsilon_{r2}$ for dielectric plate 2, and $E_{air} = (-Q/S + \sigma(t))/\varepsilon_0$ in the air gap, respectively. Here ε_0 is the vacuum permittivity, σ is the charge density at the contact surface of the tribo-pair, and S is the contact area of the tribo-pair. The voltage between the two electrodes is $V = E_1 d_1 + E_2 d_2 + E_{air} x(t)$. For the conductor-to-dielectric structure TENG, there will be no dielectric plate 2, i.e., d_2 and E_2 are zero; thus the voltage becomes $V = E_1 d_1 + E_{air} x(t)$. If we define the equivalent thickness of the dielectric plates to be $d_0 = d_1/\varepsilon_{r1} + d_2/\varepsilon_{r2}$, the V-Q-x relationship could be expressed as follows:

$$V = -\frac{Q}{S\varepsilon_0}(d_0 + x(t)) + \frac{\sigma x(t)}{\varepsilon_0} \tag{1}$$

Here, $x(t)$ is the varying gap distance between the tribo-pair due to external mechanical loading imposed to the TENG device. In special circuit conditions, for short-circuit condition with the output voltage $V = 0$, the current is $I_{sc} = \frac{dQ}{dt} = \frac{S\sigma d_0}{(d_0 + x(t))^2}\frac{dx}{dt}$; for open-circuit condition with transferred charge $Q = 0$, the voltage is $V_{oc} = \frac{\sigma x(t)}{\varepsilon_0}$.

According to Ohm's law, when the TENG is connected with a load resistance R to form a circuit, the output voltage in the circuit can be expressed as

$$V = IR = R\frac{dQ}{dt} \tag{2}$$

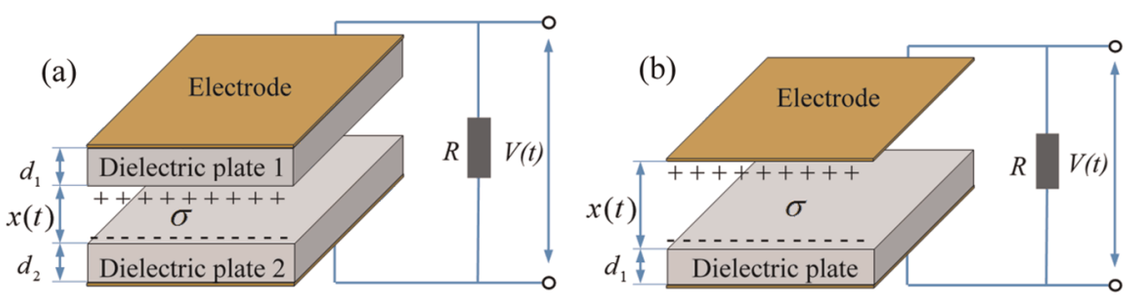

Figure 2.
Basic structure and model of the contact-mode TENG. (a) Dielectric-to-dielectric mode TENG and (b) conductor-to-dielectric mode TENG [18].

Substituting Eq. (1) into Eq. (2), we will have the equation for Q as

$$R\frac{\mathrm{d}Q}{\mathrm{d}t} = -\frac{Q}{S\varepsilon_0}(d_0 + x(t)) + \frac{\sigma x(t)}{\varepsilon_0} \tag{3}$$

With initial condition of $Q(t=0)=0$, the expression of $Q(t)$ will be

$$Q = \sigma S - \sigma S e^{-\frac{1}{RS\varepsilon_0}\left(d_0 t + \int_0^t x(t)\mathrm{d}t\right)} - \frac{\sigma}{R\varepsilon_0} e^{-\frac{1}{RS\varepsilon_0}\left(d_0 t + \int_0^t x(t)\mathrm{d}t\right)} \int_0^t d_0 e^{\frac{1}{RS\varepsilon_0}\left(d_0 z + \int_0^z x(t)\mathrm{d}z\right)}\mathrm{d}z \tag{4}$$

With the output voltage as

$$\begin{aligned} V(t) = R\frac{dQ}{dt} = &-\frac{\sigma d_0}{\varepsilon_0} + \frac{\sigma(d_0 + x(t))}{\varepsilon_0}\exp\left[-\frac{1}{RS\varepsilon_0}\left(d_0 t + \int_0^t x(t)\mathrm{d}t\right)\right] \\ &+ \frac{\sigma d_0}{\varepsilon_0}\frac{d_0 + x(t)}{RS\varepsilon_0}\int_0^t \exp\left(-\frac{d_0(t-\tau)}{RS\varepsilon_0} - \frac{1}{RS\varepsilon_0}\int_\tau^t x(z)\mathrm{d}z\right)\mathrm{d}\tau \end{aligned} \tag{5}$$

This V-Q-x relationship provides a means for evaluation of the electric output of contact-mode TENG, which may also be used for single-electrode mode TENG.

To verify the accuracy and precision of the proposed relationship, the experimental results from Ref. [16] are utilized here as an example for contact-mode TENG. Glass and polydimethylsiloxane (PDMS) are used as the tribo-pair in the experiment in planar form. The physical parameters of the device and experiment design are listed in **Table 1**. The TENG device is driven by a dynamic testing machine with separation gap $x(t)$ between tribo-pair (see **Figure 3a**, black solid line).

According to the experimental settings in Ref. [16], we introduce a piecewise function to describe the motion process of the tribo-pair as

$$x(t) = \begin{cases} 0, & 0 \le t \le (1-\eta)T, \\ A\sin\left(\dfrac{\pi t}{\eta T}\right), & (1-\eta)T < t \le T. \end{cases} \tag{6}$$

Here, η is the separation ratio representing the ratio of the separation time to the entire period. The smaller the separation ratio, the faster the tribo-pair gets into contact and thus the longer the contact time. In each period, the dielectric plates are supposed to start the charging process which occupies the time period from 0 to $(1-\eta)T < t \le T$ when the tribo-pair keeps contact ($x = 0$).

Parameter	Value
Thickness of PDMS plate d_1	100 μm
Relative permittivity of PDMS ε_{r1}	2.7
Thickness of glass d_2	1 mm
Relative permittivity of glass ε_{r2}	7.2
Permittivity of vacuum ε_0	8.854×10^{-12} F/m
Area of the dielectrics S	25 cm^2
Surface charge density σ	5–40 $\mu C/m^2$

Table 1.
Parameters of contact-mode TENG [16].

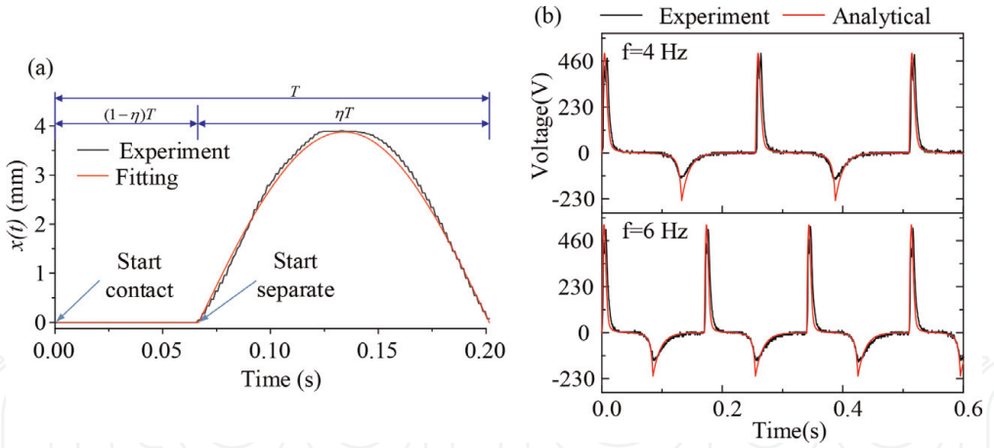

Figure 3.
(a) Oscillation scheme used in experiment (black line) and its fitting function that is input into the analytical solution (red line) and (b) comparisons of the theoretical predictions on output voltage with experimental measurements [25].

In **Figure 3b**, the voltage output obtained by Eq. (5) is compared with the experimental results from Ref. [16]. Excellent agreements could be observed between the experimental and analytical results due to different loading frequencies, especially the positive part of the voltage output. For the negative part of the results, the analytical results are slightly larger than the experimental ones, particularly for the low contact frequency case. The results presented above clearly indicate the accuracy of the model and method developed in this work.

2.1.2 Sliding-mode TENG

For lateral sliding-mode TENG, the basic structure is shown in **Figure 4**.

For the lateral sliding-mode TENG, the contact area is S, the sliding distance is $x(t)$, the length of the tribo-pair is l, and the width is w. Since l is always much larger than d_1 and d_2 as the tribo-pair, and x is always smaller than $0.9l$, it is difficult to keep tribo-pair in perfect alignment. In this condition, the total capacitance C can be estimated as $C = \varepsilon_0 w(l-x)/d_0$. Utilizing the charge distribution shown above and Gauss theorem, the V_{oc} can be estimated as $V_{oc} = \sigma x d_0/\varepsilon_0 w(l-x)$. So the V-Q-x relationship can be shown as

$$V = -\frac{Q}{C} + V_{oc} = -\frac{Qd_0}{\varepsilon_0 w(l-x)} + \frac{\sigma x d_0}{\varepsilon_0 w(l-x)} \tag{7}$$

For conductor-to-dielectric TENGs when the edge effect can be neglected, the relationship is similar by turning d_2 into zero. As a result, we can get the output voltage of sliding-mode TENG as

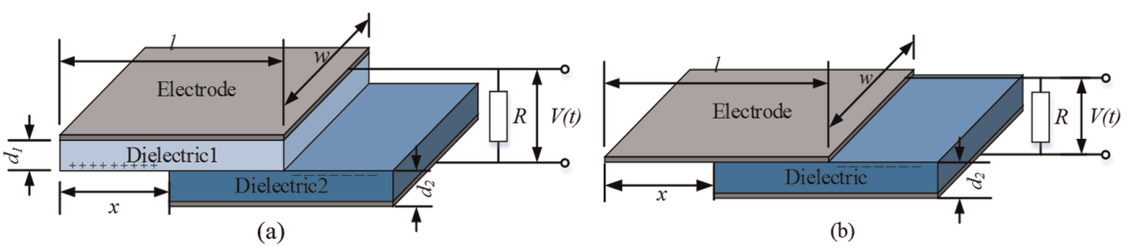

Figure 4.
Theoretical model of sliding-mode TENG. (a) Dielectric-to-dielectric sliding-mode TENG and (b) conductor-to-dielectric sliding-mode TENG [26].

$$V = \frac{\sigma d_0}{\varepsilon_0}\left[\frac{l}{l-x(t)}\exp\left(-\frac{d_0}{\varepsilon_0 RS}\int_0^t \frac{l}{l-x(t)}\mathrm{d}t'\right) + \frac{d_0}{\varepsilon_0 RS}\frac{l}{l-x(t)}\int_0^t \exp\left(\frac{d_0}{\varepsilon_0 RS}\int_t^{t'} \frac{l}{l-x(\delta)}d\delta\right)\mathrm{d}t' - 1\right] \tag{8}$$

Based on these output voltage expressions, we can get the average power output for TENG as

$$P_{\text{eff}} = \frac{1}{T}\int_t^{t+T} \frac{V^2}{R}\mathrm{d}t \tag{9}$$

Here, T is the time span of one mechanical loading cycle.

This V-Q-x relationship provides a method for evaluation of the electric output of sliding-mode TENG, which may be easily extended as a methodology for sliding freestanding tribo-layer mode TENG. To make sure the accuracy and precision of the proposed V-Q-x relationship of sliding-mode TENG, the experiments from Ref. [17] are carried out for validation. The materials and scale parameters are shown in **Table 2**.

In the experiments, the tribo-pair is fixed on a horizontal tensile loading platform for reciprocating lateral sliding process. The sliding process of the tribo-pair was imposed by the dynamic testing machine with a symmetric acceleration-deceleration mode (**Figure 5c**). The analytical results of the voltage output obtained by Eq. (8) agree very well with the experimental result.

Based on the V-Q-x relationships presented from Eqs. (5)–(8), the output performance of TENG is predictable when device structure, material parameters, and motion process are clear. With these equations, the influence of each parameter is clear, while all others are certain. For example, we can change the one parameter such as load resistance while all the others kept unchanged. As a result, we can get the output characteristic of the target TENG device and find out the optimized load resistance.

With this method, parametric analyses are carried out to characterize the output performance of TENGs with different working conditions. Niu et al. studied the output characteristics of contact-mode [18], sliding-mode [19], single-electrode

Parameter	Value
Dielectric tribo-pair	PTFE-nylon
Thickness of nylon plate d1 (μm)	50
Relative permittivity of Nylon εr1	4
Thickness of PTFE plate d2 (μm)	50
Relative permittivity of PTFE εr2	2.1
Permittivity of vacuum ε0 (F/m)	8.854×10^{-12}
Area of the dielectrics S (m^2)	0.05×0.071
Surface charge density σ (μCm^{-2})	200
Maximum separate distance A (m)	0.05
Acceleration a (m/s^2)	20
Load resistance R (MΩ)	10–1000

Table 2.
Parameters of sliding-mode TENG [17].

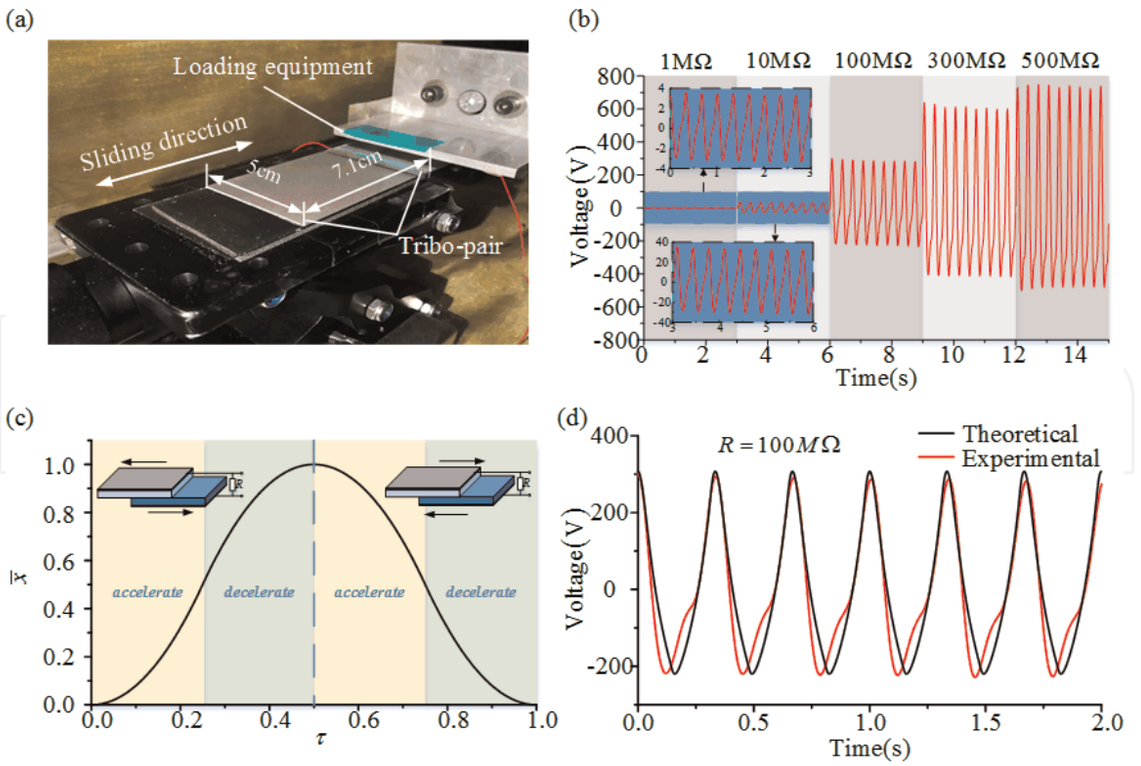

Figure 5.
(a) The TENG device in testing, (b) time history of output voltage, (c) simulation of dimensionless sliding process and (d) comparison of time history of output voltage between theoretical results and experimental results [26].

mode [20], and freestanding-mode [21] TENG under different load resistances, products of velocities, contact area sizes, effective dielectric thicknesses, and gap distances. These works obtained the effect of a series of independent parameters on the output characteristics including load resistance, maximum gap or slid distance, moving speed, device capacitance, and device structure parameters. These works, by numerical calculation of the real-time output characteristics, presented the suitable value range of these preceding parameters with common TENG device design and provided excellent guidance for structural design and optimization strategies for TENG devices.

2.2 Optimization approach based on figure of merit

For various applications, four basic modes of TENGs have been developed. Each mode has its own structure and various triboelectric material choices for the tribo-pair. That makes it difficult to characterize and compare the output performance of TENG. A universal standard has to be introduced to quantify the performance of the TENGs, regardless of its operation mode. To solve this problem, the figure of merit of TENG is proposed [22]. It gives a quantitative evaluation of TENG's performance from both structure's and the materials' points of view [22–24]. The application of figure of merit leads to a more efficient design and optimization approach of various TENG structures in practical applications. It may help to establish a series of standards for developing TENGs toward practical applications and industrialization.

The figure of merits of TENG includes performance figure of merit related to the structure and material figure of merit related to surface charge density. The theoretical derivation and simulation of these two figures of merit will be discussed in Sections 2.2.1 and 2.2.2, respectively.

2.2.1 Figure of merit for quantifying the output performance of TENG

Based on the V-Q-x relationship, a series of optimization strategies for independent parameters have been proposed. But their optimization target is the maximum output voltage or power, and the physical properties of the tribo-pair are not taken into account. To take into consideration the influence of other parameters of the device, the performance figure of merit (FOM_P) is developed as a new standard. It stands for the maximum power density of TENG, which represents a quantitative standard to reflect the output capability of TENGs with different configurations [22]. The expression of FOM_P is

$$\mathrm{FOM_P} = 2\varepsilon_0 \frac{E_m}{Ax_{\max}} \tag{10}$$

Here, E_m is the largest possible output energy per cycle, $x_{\max}$ is the maximum displacement of tribo-pair, and A is the contact area. The FOM_P is considered as a universal standard to evaluate varieties of TENGs, since it is directly proportional to the greatest possible average output power regardless of the mode and size of TENG [22]. To obtain the FOM_P, the power output per cycle of TENG is required first.

The output energy per cycle E can be calculated through the encircled area of the closed loop in the V-Q curve as

$$E = \overline{P}T = \int_0^T VI\mathrm{d}t = \int_{t=0}^{t=T} V\mathrm{d}Q = \oint V\mathrm{d}Q \tag{11}$$

The V-Q curve is usually obtained from the working process of TENG by the V-Q-x relation. In general, the working process of any type of TENG contains four steps as a cycle (**Figure 6a**). As **Figure 6b** shows, the V-Q curve becomes steady after a few initial cycles. The output energy per cycle derived from these steady periodic cycles is named as "cycles for energy output" (CEO).

For each CEO, the difference between the maximum and the minimum transferred charges in its steady state is defined as the total cycling charge Q_C. As **Figure 6b** shows, Q_C is always smaller than the maximum transferred charge $Q_{SC.max}$. If the Q_C could be maximized to $Q_{SC.max}$, we may achieve the maximum power output. Having noticed that the $Q_C = Q_{SC.max}$ only occurs in short-circuit condition, we add a switch in parallel with the external load and design the following repeated steps to achieve instantaneous short-circuit conditions during operations: step 1, the tribo-pair separates from $x = 0$ to $x = x_{max}$at switch off; step 2, turn switch on to enable $Q_C = Q_{SC.max}$; step 3, the tribo-pair displaces from $x = x_{max}$ to $x = 0$ at switch off; and step 4, turn the switch on to enable $Q_C = 0$. With this process, we may obtain the V-Q plot in **Figure 6c**. These cycles are named "cycles for maximized energy output" (CMEO) by Ref. [22].

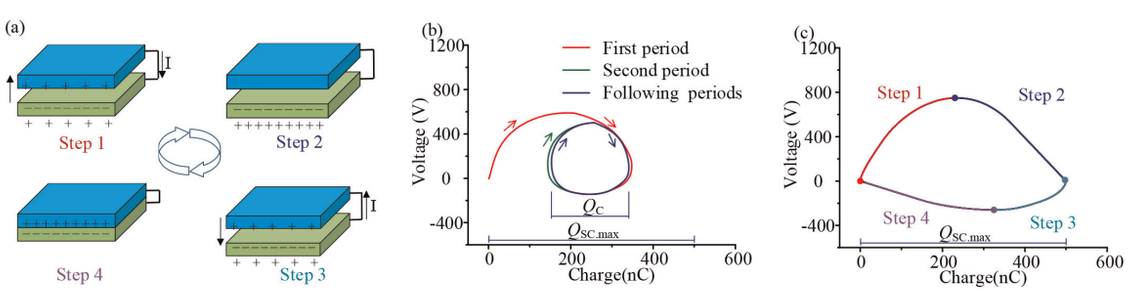

Figure 6.
(a) Working process of TENG, (b) voltage-charge (V-Q) plot for CEO, and (c) V-Q plot for CEMO [22].

The CMEO is related to load resistance of the output circuit: the higher the resistance, the higher the output energy per cycle. Therefore, the maximized output energy could be obtained when an infinitely large resistor as

$$E_m = \frac{1}{2} Q_{\mathrm{SC.max}} \left(V_{\mathrm{OC.max}} + V'_{\mathrm{max}} \right) \tag{12}$$

Here $Q_{\mathrm{SC.max}}$ is the short-circuit transferred charge, $V_{\mathrm{OC.max}}$ is the maximum open-circuit voltage, and V'_{max} is the maximum achievable absolute voltage. The equation for E_m of TENG operated in any conditions can also be expressed as

$$E_m = \int_0^{t_1} P_1(t)\mathrm{d}t + \int_{t_1}^{t_2} P_2(t)\mathrm{d}t + \int_{t_2}^{t_3} P_3(t)\mathrm{d}t + \int_{t_3}^{t_4} P_4(t)\mathrm{d}t \tag{13}$$

The average power output $\overline{P}$ is then

$$\overline{P} = \frac{E_m}{T} \approx \frac{\overline{v} E_m}{2x_{\mathrm{max}}} \tag{14}$$

Here $\overline{v}$ is the average velocity of the relative motion in tribo-pair. Thus, we can define the $\mathrm{FOM_P}$ depending on the parameters of E_m, x_{max}, and A and get its expression as Eq. (10).

2.2.2 Figure of merit for quantifying material characteristic

From Section 2.1, we notice that the transfer charge Q and output voltage V are proportional to the surface charge density σ in the V-Q-x relations of TENG. The increase of σ will directly enhance the possible average output power of TENG significantly as the power output is proportional to σ^2. Yet for $\mathrm{FOM_P}$ as Eq. (10) shows, the material characteristic is not taken into consideration. Thus we define the material figure of merit ($\mathrm{FOM_m}$) as a standard to quantify the charge density of general surface as

$$\mathrm{FOM_m} = \sigma^2 \left(\mathrm{C^2/m^4} \right) \tag{15}$$

The $\mathrm{FOM_m}$ is only determined by σ and the component related to the material properties alone. It can be used to evaluate the triboelectric performance of the materials in contact [22].

The accurate value of σ for one kind of material is measured by putting it into a testing TENG device and using electrometer to measure the total transfer charge. To avoid the influence of uncertain contact conditions, the testing TENG device utilizes liquid metals as the other material of the tribo-pair to get the maximum possible surface charge of the material. Through this method, the $\mathrm{FOM_m}$ of a series of commonly used materials has been acquired, and their position in triboelectric series compared with the liquid metal has been figured out. These results in detail can be found in Ref. [22] and its following works.

2.2.3 Application of figure of merits

The figure of merits provides a series of quantitative standards to evaluate the working performance of TENG. Their application enables more efficient design and optimization of various TENGs in practical applications. The optimization works based on figure of merits are likely to establish the principles for TENG design and develop TENGs toward practical applications and industrialization.

Through FOM_P, we introduced a universal standard to quantify the power output performance of the TENG regardless of its operation mode and materials. With this standard, we are able to evaluate the performance of the TENGs in different structures/modes and achieve the optimization approach for structure design and working parameter setting. Using Eq. (11), we may obtain the FOM_P for different TENGs with same tribo-pair and contact area through analytical and simulation method. Taking the maximum FOM_P as an optimization index, we will achieve the optimized structure/mode for a TENG. On the other hand, for a known TENG, we can find out its maximum FOM_P and thus determine the best suitable working condition like load resistance, x_{max}, etc. Through these analyses based on FOM_P, the following conclusions have been found: (1) x_{max} influences the output of TENG directly, and when x_{max} grows, the total transferred charges will increase and so does the output power; (2) the power output performance of TENG triggered by contact-separation action is better than that of sliding action; and (3) reducing the parasitic capacitance can help to increase the power output of TENG, and also larger-area generators with larger air gap capacitance are much more robust to parasitic leakage [22–24].

Using FOM_m, we have introduced a quantitative standard to evaluate the maximum surface charge density for a triboelectric material. With FOM_m of different materials, we are able to determine their triboelectric charge polarity. And with different FOM_m of tribo-pairs, we can find the optimal choice for a TENG. With this standard, we found some useful regulations: (1) the optimized choice of materials in a tribo-pair should be in opposite polarities, and (2) the larger the polarity differential between the materials, the bigger the FOM_m of the tribo-pair [22].

2.3 Optimization strategy for TENG based on multiparameter analysis

For TENGs, their electric output performance is simultaneously and coherently influenced by a group of factors including the dimensions of the electrodes and insulators, electrical properties of the materials and the loading processing, etc. These parameters are interlinked with each other; therefore changing one parameter with the others fixed may break the optimized condition of the device and require new adjustment in other parameters and further optimization. It is necessary to simulate the output performance of a TENG via theoretical models based on multiparameter analysis rather than specific cases with only one variable considered. In addition, TENGs could be used as sensor or energy harvester in either macro- or microscale, within which the physical properties of materials and device are quite different. Hence, the dimensionless analysis method is more feasible for parameter analysis of TENG.

Here, to realize the optimization of the device, we developed a series of normalized expressions for output voltage and output power in dimensionless forms, which provide a group of scaling laws between the normalized electric output and two independent compound variables. These scaling laws can facilitate the analysis of the effects in different aspects of the device simultaneously and provide accordance for optimal design of TENG by considering the effects of all factors simultaneously. The optimal electric output could be obtained through the proposed formulations with all parameters of the TENG considered as variables [25, 26].

2.3.1 Contact-separation mode TENG

For the optimization of contact-separation mode TENG, a set of expressions for normalized electric voltage and power in dimensionless forms are proposed in this section. In these dimensionless expressions, the effects of all the parameters

involved have been investigated comprehensively and simultaneously. The normalized expressions for output voltage and power may facilitate the optimization based on the scaling laws by tuning different physical properties simultaneously rather than those only focusing on one physical property either in dimensional or dimensionless forms [25].

For the output voltage in a general circuit with the load resistance of R, the various structure, material, mechanical loading, and circuit properties of TENG are investigated in a coherent manner and expressed with two combined parameters. The dimensionless expression for normalized output voltage that depends only on the two combined parameters is derived based on Eq. (5) as

$$\frac{V(\tau)\varepsilon_0}{\sigma A} = \overline{V}_A\left(\tau, \frac{A}{d_0}, \frac{RS\varepsilon_0}{AT}\right) = -\frac{d_0}{A} + \left(\frac{d_0}{A} + \overline{x}(\tau)\right)\exp\left[-\frac{AT}{RS\varepsilon_0}\left(\frac{d_0}{A}\tau + \int_0^\tau \overline{x}(\tau)d\tau\right)\right]$$
$$+\frac{AT}{RS\varepsilon_0}\frac{d_0}{A}\left(\frac{d_0}{A} + \overline{x}(\tau)\right)\int_0^\tau \exp\left[\frac{AT}{RS\varepsilon_0}\left((\zeta-\tau)\frac{d_0}{A} + \int_\tau^\zeta \overline{x}(\zeta)d\zeta\right)\right]d\zeta \tag{16}$$

where $\tau = t/T$ is the dimensionless time and A and T are, respectively, the oscillation amplitude and the period of the separation-contact cycle.

While for the application of energy harvest, the output power should be a key variable for characterizing the performance of the generator. According to the definition of output power $P_{\text{eff}} = \frac{1}{R}\sqrt{\frac{\int_0^T V^2(t)\mathrm{d}t}{T}}$, the dimensionless output power may be given by

$$\frac{P_{\text{eff}}T\varepsilon_0}{\sigma^2 AS} = \overline{P}_A\left(\frac{A}{d_0}, \frac{RS\varepsilon_0}{AT}\right) \tag{17}$$

Here, we can see that the dimensionless output voltage and power depend only on two combined parameters, i.e., A/d_0 and $RS\varepsilon_0/AT$, in which A/d_0 characterizes the relative oscillation amplitude, while $RS\varepsilon_0/AT$ reflects the hybrid effects of generator area, electrical resistance, oscillation amplitude, and period of the tribo-pair. Besides this universal optimization of TENG by tuning multiple parameters at the same time, we may still realize the optimization for individual physical quantity with the assumption of other parameters fixed. However, we cannot figure out how to optimize the oscillation amplitude A to achieve the peak output from Eqs. (16) and (17) since this physical property get involved in both the combined dimensionless parameter and the normalized electric output. For the same reason, we may not work out the effect of the generator area S and the mechanical loading period T on the output power with Eq. (17).

If we want to examine the effect of S on the output power, we may simply multiply Eq. (17) with the factor $RS\varepsilon_0/AT$ and have

$$\frac{P_{\text{eff}}R\varepsilon_0^2}{\sigma^2 A^2} = \overline{P}_{AR}\left(\frac{A}{d_0}, \frac{RS\varepsilon_0}{AT}\right) \tag{18}$$

To investigate the effect of oscillation amplitude and period, another set of dimensionless expressions is derived by multiplying Eqs. (16) and (17) with the factor A/d_0 and the combined parameter $RS\varepsilon_0/AT$ and multiplying Eq. (18) with A^2/d_0^2 and $RS\varepsilon_0/AT$. This set of dimensionless expressions for the scaling laws will be

$$\frac{V(\tau)\varepsilon_0}{\sigma d_0} = \overline{V}_d\left(\frac{A}{d_0}, \frac{RS\varepsilon_0}{d_0 T}\right) = -1 + \left(1 + \frac{A}{d_0}\overline{x}(\tau)\right)\exp\left[-\frac{d_0 T}{RS\varepsilon_0}\left(\tau + \frac{A}{d_0}\int_0^{\tau}\overline{x}(\tau)d\tau\right)\right] + \frac{d_0 T}{RS\varepsilon_0}\left(1 + \frac{A}{d_0}\overline{x}(\tau)\right)\int_0^{\tau}\exp\left[\frac{d_0 T}{RS\varepsilon_0}\left((\zeta - \tau) + \frac{A}{d_0}\int_{\tau}^{\zeta}\overline{x}(\zeta)d\zeta\right)\right]d\zeta \tag{19}$$

$$\frac{P_{\text{eff}} T\varepsilon_0}{\sigma^2 d_0 S} = \overline{P}_d\left(\frac{A}{d_0}, \frac{RS\varepsilon_0}{d_0 T}\right) \text{ or } \frac{P_{\text{eff}} R\varepsilon_0^2}{\sigma^2 d_0^2} = \overline{P}_{dR}\left(\frac{A}{d_0}, \frac{RS\varepsilon_0}{d_0 T}\right) \tag{20}$$

The relations in Eqs. (16)–(20) also reveal that the effective output voltage (or power) is proportional to the square of surface charge density. These dimensionless parameters and corresponding scaling laws also show a straightforward optimization method for the magnitude of oscillation at the same electrical load resistance, generator area, or oscillation period.

To verify the dimensionless expressions, we compare the peak dimensionless output voltage based on Eqs. (16) and (19) with the experimental results in corresponding dimensionless forms. Two groups of experiments with various thicknesses d_{glass} of glass plate [16] are utilized for comparisons. In Group I, the oscillation frequency $1/T$ varies from 1 Hz to 6 Hz with the load resistance fixed at $R = 100\ \ M\Omega$, while in Group II, the load resistance R varies from 1 MΩ to 1000 MΩ with the oscillation frequency fixed at $1/T = 5$ Hz. The theoretical predictions for the dimensionless voltage $V_{\text{peak}}\varepsilon_0/\sigma A$ and $V_{\text{peak}}\varepsilon_0/\sigma d_0$ (solid lines) both agree very well with experiments (markers) in **Figure 6**.

As can be seen from **Figure 7**, the theoretical predictions agree very well with the experimental measurements despite that the latter are achieved with different device structures, mechanical loadings, and circuit conditions. This demonstrates that the established scaling law reveals the underlying general correlation between the physical properties of the device and its output performance, which may provide robust guidelines for optimization strategies, no matter what way we use to make it, theoretical or experimental. Take the varying parameters T and R in the two experimental groups as an instance: from the experimental point of view, they are totally different parameters, of which the variations affect the output performance, respectively. However, we find in the scaling law the unified expression for the two parameters in $RS\varepsilon_0/AT$ (or $RS\varepsilon_0/d_0 T$). The individual variation of either T or R has since become the variation of the compound variables. That is to say, the same compound variable may have different combinations of T and R. According to the scaling laws shown in Eqs. (16)–(20), the output voltages should have the same value in the cases with the same compound variables $RS\varepsilon_0/AT$ (or $RS\varepsilon_0/d_0 T$) and A/d_0 even if the latter are comprised of parameters valued with different combinations. It indicates the necessity for coupling design of these parameters included in the compound variables to achieve the best output performance of the device.

However, the correlations among the parameters and their simultaneous effect on the output performance are hard to be found in traditional optimization techniques based on single-parameter investigations, in neither experimental nor theoretical means. As thus, we can conclude that the scaling law proposed in this paper can be not only used to predict the output performance of a TENG comprehensively and systematically with all parameters being considered simultaneously but also treated as a general and rational optimization criterion for the device toward its best performance. Based on the scaling laws from Eqs. 16 to 20, the output performance of the generator can be optimized by tuning combined parameters or individual physical quantities. The scaling law for the output voltage and power in a form of either in Eqs. (16)–(18) or in Eqs. (19)–(20) provide a universal optimizing strategy

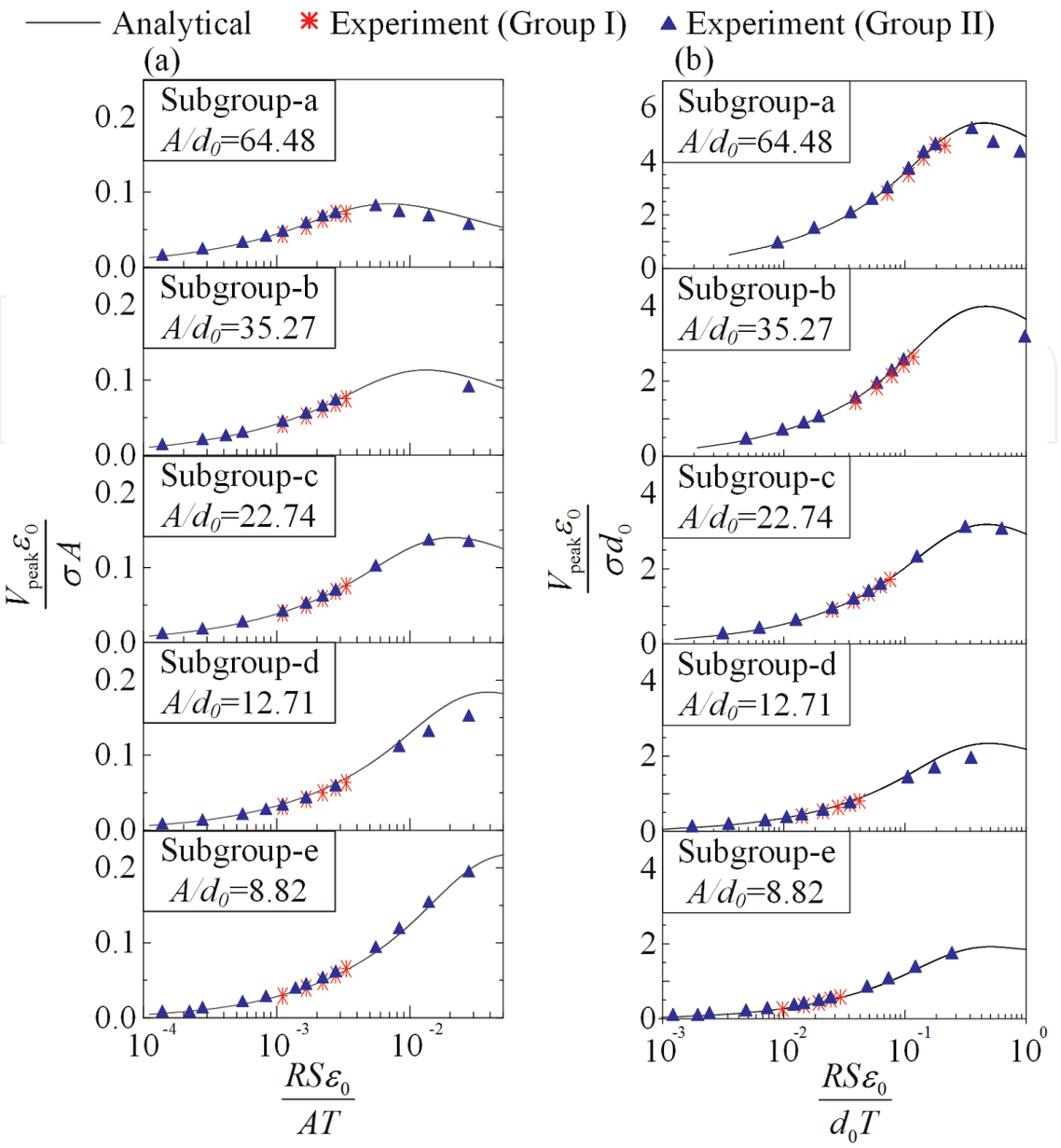

Figure 7.
Validation of the scaling laws for dimensionless peak output voltage through comparisons with experimental measurements with different setups [25].

to enhance the output voltage for sensing application or maximum output power for energy harvesting application [25].

In **Figure 8**, the maximum peak voltage is obviously increasing monotonically with the relative oscillation amplitude A/d_0 (**Figure 8a**). While for each given value of A/d_0, there exists an optimized $RS\varepsilon_0/AT$ that delivers a maximum dimensionless output power (**Figure 8b**). It suggests that we may achieve the best output performance of TENG through tuning multiple physical parameters simultaneously. From **Figure 8**, we can also find that the pinpoint for a peak output power or power density (=0.25) is located around $A/d_0 = 2.0$ and $RS\varepsilon_0/AT = 0.12$.

Besides the universal optimization with multiple parameters, we may also use individual parameter analysis by tuning its quantity to enhance the output performance. For instance, from **Figure 8b** it is found that given all other parameters, there exists an optimal load resistance to achieve a maximum output power. While from **Figure 8c** with given load resistance and oscillation amplitude, it can be found that larger generator area and higher oscillation frequency may enhance the output power until saturated.

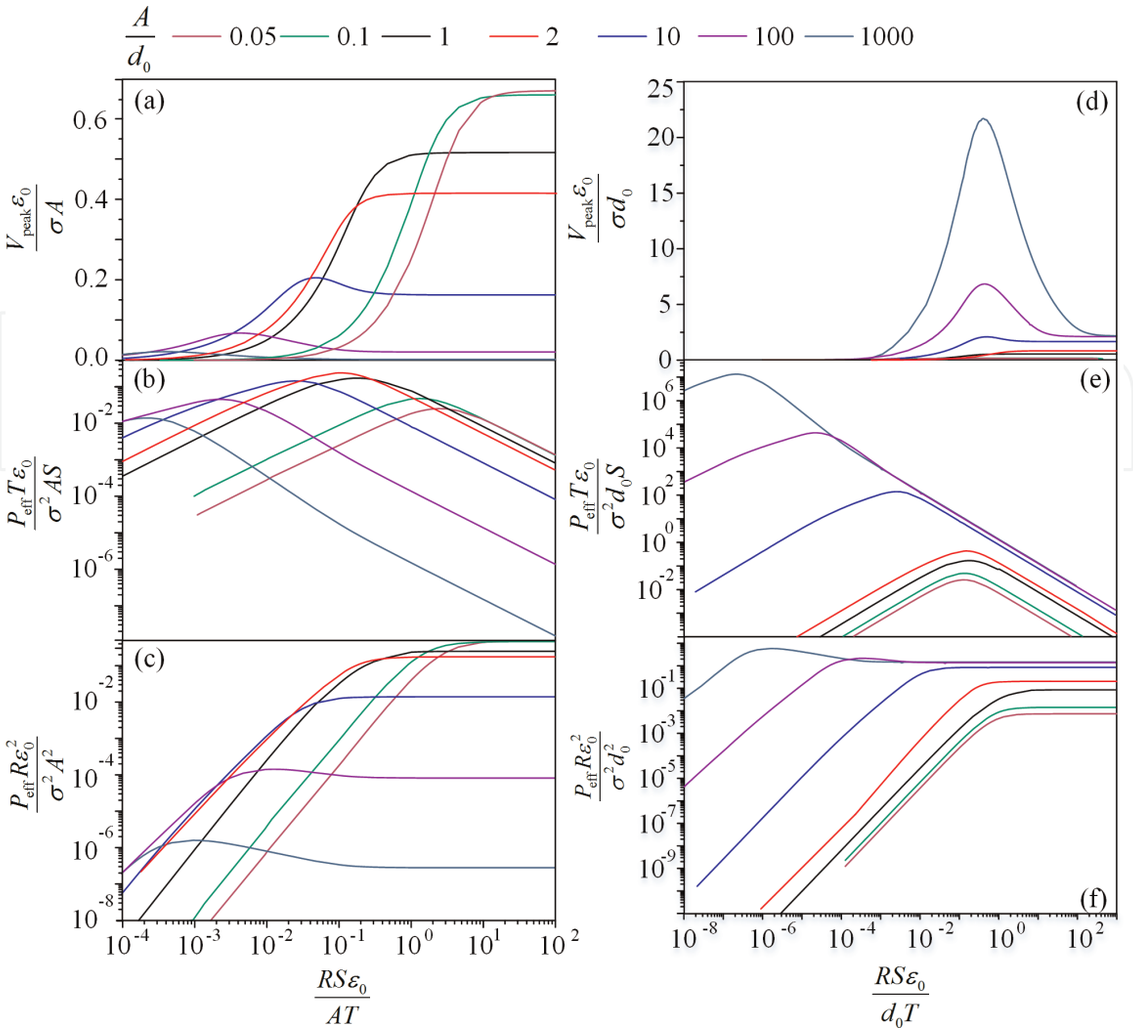

Figure 8.
Scaling laws for peak output voltage and output power [25].

As mentioned before, the scaling laws in Eqs. (16)–(19) cannot reflect a clear dependence of the output performance on the oscillation amplitude A since it is included in both two dimensionless parameters. Fortunately, with the scaling laws in Eqs. (20) and (21), the effect of A is extracted and can be distinguished quantitatively from the numerical results. **Figure 8e–f** shows that increasing the oscillation amplitude may enhance the output power or power density monotonically and only a smaller generator area, lower oscillation frequency, or load resistance may achieve an optimized output power [25].

2.3.2 Sliding-mode TENG

For the optimization of sliding-mode TENG, Zhang [26] established a series of dimensionless expressions of output performance of sliding-mode TENG according to Eq. (7) as

$$\overline{V}_R\left(\tau,\frac{A}{l},\frac{\varepsilon_0 RS}{d_0 T}\right)=\frac{\varepsilon_0 V(\tau)}{\sigma d_0}=\frac{1}{1-\frac{A}{l}\overline{x}(\tau)}\exp\left(-\frac{d_0 T}{\varepsilon_0 RS}\int_0^{\tau}\frac{1}{1-\frac{A}{l}\overline{x}(\tau')}\tau'\right)$$
$$+\frac{d_0 T}{\varepsilon_0 RS}\frac{1}{1-\frac{A}{l}\overline{x}(\tau)}\int_0^{\tau}\exp\left(\frac{d_0 T}{\varepsilon_0 RS}\int_{\tau}^{\tau'}\frac{1}{1-\frac{A}{l}\overline{x}(\delta)}d\delta\right)d\tau'-1 \tag{21}$$

Here, A is the maximum sliding distance. When used as energy harvesters, the output power will become the key target to evaluate the output characteristics of TENG. According to the definition of effective output power, the dimensionless output power can be expressed as

$$\overline{P}_T\left(\frac{A}{l},\frac{\varepsilon_0 RS}{d_0 T}\right)=\frac{\varepsilon_0^2 R P_{\text{eff}}}{\sigma^2 d_0^2}=\int_0^1 \overline{V}^2 d\tau \tag{22}$$

In Eqs. (21) and (22), there are two dimensionless compound parameters A/l and $\varepsilon_0 RS/d_0 T$ affecting the dimensionless output characteristics of device, which could be described with a group of parameters related to various aspects of TENG device. From these equations, we may understand the effects of the load resistance R, planer area S, loading period T, and maximum sliding distance A on output voltage at the same time. Similarly, based on Eq. (23), we can figure out the optimized parameters for power improvement. Meanwhile, the dimensionless expressions also reflect the relationship between the compound parameters (A/l and $\varepsilon_0 RS/d_0 T$) and the output performance.

To make the normalized output performance better understood from the physical point of view, they can also be described with the dimensionless capacitance $\overline{C}$ and the dimensionless time constant $\overline{T}$, in which the expression for $\overline{C}$ is $\overline{C}=C_A/C_0=1-A/l$, with $C_0=\varepsilon_0 S/d_0$ the capacitance when $x=0$ and $C_A=C(x=A)=\varepsilon_0 S(1-A/l)/d_0$ the equivalent capacitance of the device when $x=A$. Here $\overline{C}$, from the physical point of view, represents the ratio of the capacitance with $x=A$ to the capacitance with $x=0$. The dimensionless time constant is defined as $\overline{T}=RC_0/T=\varepsilon_0 RS/d_0 T$, which reflects the time constant for the first-order circuits with $C=C_0$ to the period of the alternating current. The expression for normalized output voltage versus $\overline{C}$ and $\overline{T}$ is

$$\begin{aligned}\overline{V}_R(\tau,\overline{C},\overline{T})=\frac{\varepsilon_0 V(\tau)}{\sigma d_0}&=\frac{1}{1-(1-\overline{C})\overline{x}(\tau)}\exp\left(-\frac{1}{\overline{T}}\int_0^\tau\frac{1}{1-(1-\overline{C})\overline{x}(\tau')}d\tau'\right)\\&+\frac{1}{\overline{T}}\frac{1}{1-(1-\overline{C})\overline{x}(\tau)}\int_0^\tau\exp\left(\frac{1}{\overline{T}}\int_\tau^{\tau'}\frac{1}{1-(1-\overline{C})\overline{x}(\delta)}d\delta\right)d\tau'-1\end{aligned} \tag{23}$$

$$\overline{P}_T(\overline{C},\overline{T})=\frac{\varepsilon_0^2 R P_{\text{eff}}}{\sigma^2 d_0^2}=\int_0^1 \overline{V}_R^2(\tau)d\tau \tag{24}$$

Similar to Eqs. (16)–(18) of contact-mode TENG, in this circumstance, the influence of d_0 on normalized output voltage is not reflected in Eq. (23), neither the effects of d_0 and R on normalized output power from Eq. (24). To find out the influence of these parameters, we propose the following set of expressions for normalized output voltage and power equations as

$$\begin{aligned}\overline{V}_d(\tau,\overline{C},\overline{T})=\frac{TV(\tau)}{\sigma RS}&=\frac{1}{\overline{T}}\frac{1}{1-(1-\overline{C})\overline{x}(\tau)}\exp\left(-\frac{1}{\overline{T}}\int_0^\tau\frac{1}{1-(1-\overline{C})\overline{x}(\tau')}d\tau'\right)\\&+\frac{1}{\overline{T}^2}\frac{1}{1-(1-\overline{C})\overline{x}(\tau)}\int_0^\tau\exp\left(\frac{1}{\overline{T}}\int_\tau^{\tau'}\frac{1}{1-(1-\overline{C})\overline{x}(\delta)}d\delta\right)d\tau'-\frac{1}{\overline{T}}\end{aligned} \tag{25}$$

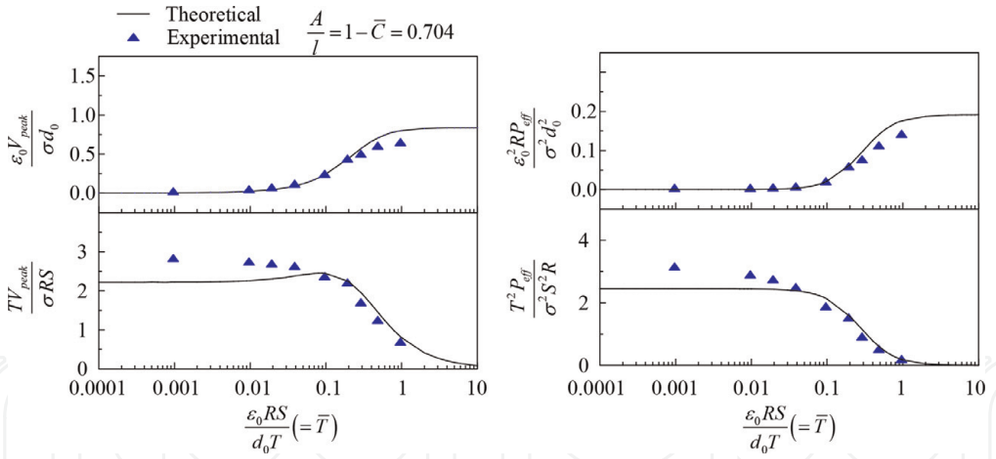

Figure 9.
Comparisons of dimensionless voltage and power between theoretical results and experimental results [26].

$$\overline{P}_d(\overline{C},\overline{T}) = \frac{T^2 P_{\text{eff}}}{\sigma^2 S^2 R} = \frac{1}{\overline{T}^2}\int_0^1 \overline{V}_R^2(\tau)d\tau \tag{26}$$

$$\overline{P}_R(\overline{C},\overline{T}) = \frac{\varepsilon_0 T P_{\text{eff}}}{\sigma^2 d_0 S} = \frac{1}{\overline{\overline{T}}}\int_0^1 \overline{V}_R^2(\tau)d\tau \tag{27}$$

These equations provide the optimal strategy for TENG design with the two compound parameters related to the TENG device. We may use these equations to study the physical interpretation of dimensionless expressions through the dimensionless capacitance and the dimensionless time constant.

To verify the dimensionless expressions, we compare the theoretical results with the experimental measurements using the peak output voltage in dimensionless forms [17]. The corresponding parameters used in experiment and simulation are listed in **Table 2**.

As **Figure 9** shows, compared with the experimental results, the theoretical curves based on scaling laws exhibit good consistent tendency with the experimental data points.

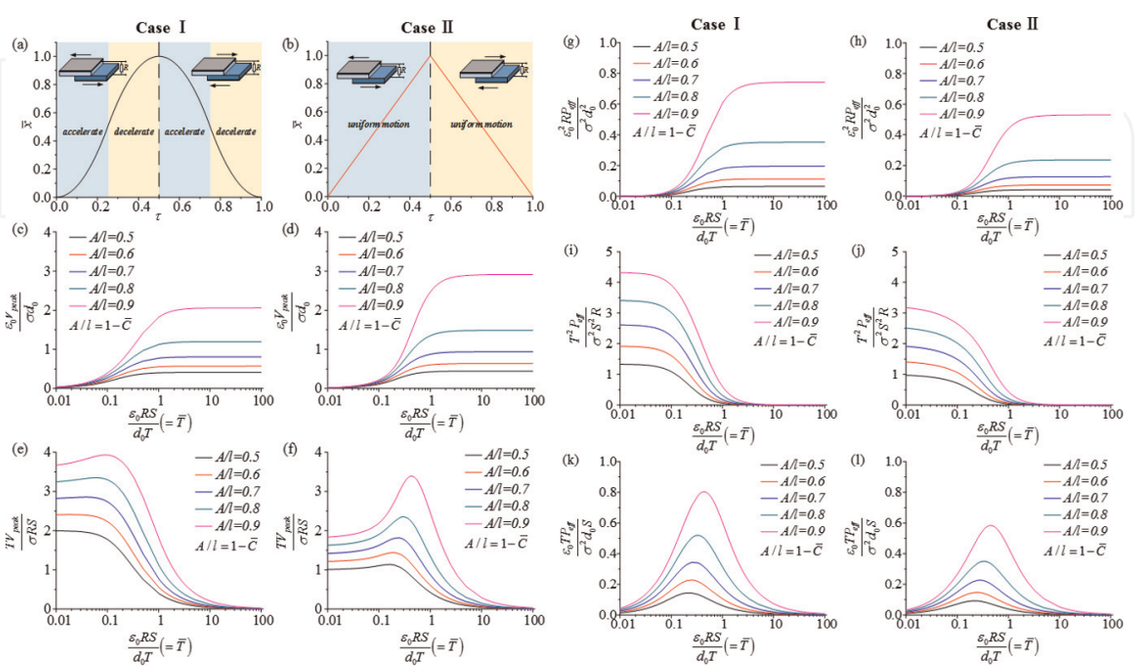

Figure 10.
Scaling laws for dimensionless output voltage and power in case I and case II [26].

According to the referring experiments [17], we define the two different forms of sliding process to simulate different mechanical loading conditions, including parabolic (Case I) and triangular (Case II) loading pattern. Based on the scaling laws for the correlation between the normalized output performance and the dimensionless compound parameters, some general optimization strategies will be acquired to improve the electric output with Eqs. (23)–(27).

From **Figure 10**, the optimal combination of A/l and $\varepsilon_0 RS/d_0 T$ for the best output performance for TENG is found, thus providing a general guideline for device optimization. In addition, we can improve the dimensionless output performance by tuning compound parameters as well as single parameter. We can also use the scaling law from another physical point of view by reflecting the output performance with the dimensionless capacitance $\overline{C}$ and time constant $\overline{T}$. The value of $\overline{C}$ and $\overline{T}$ with regard to the best output performance provides the optimization strategy for dimensionless capacitance and time constant.

From **Figure 10**, it is also obvious that increasing A/l may enhance both the peak output voltage and the maximum output power of TENG. It indicates that the larger the ratio of the maximum sliding distance to the length of the device, the higher the output performance is of the TENG. Additionally, it is found that the optimization strategies for TENG with these two different loading patterns are similar because the scaling laws between output performance and compound parameters in Cases I and II show the same trend.

In **Figure 10(c–d)**, for each A/l, the value of $\varepsilon_0 V_{\text{peak}}/\sigma d_0$ increases monotonically with $\varepsilon_0 RS/d_0 T$ and approaches to a constant when $\varepsilon_0 RS/d_0 T = 1.0$, which implies that the optimal combination $\varepsilon_0 RS/d_0 T$ is over 1. As mentioned before, the scaling laws shown in **Figure 10(c–d)** may not reflect the explicit relationships between output voltage and equivalent thickness d_0, because d_0 is included in both $\varepsilon_0 V_{\text{peak}}/\sigma d_0$ and $\varepsilon_0 RS/d_0 T$. To achieve the influence of d_0, another scaling laws are exhibited in **Figure 10(e–f)** with Eqs. (23) and (25). Instead of d_0 in **Figure 10(c–d)**, load resistance R, area S, and period T in **Figure 10(e–f)** are involved in both $TV_{\text{peak}}/\sigma RS$ and $\varepsilon_0 RS/d_0 T$, which means the effect of R, S, and T on output voltage may not be reflected in **Figure 10(d–f)**. For each A/l, a peak value of $TV_{\text{peak}}/\sigma RS$ is found, which indicates the existence of the optimal $\varepsilon_0 RS/d_0 T$ or $\overline{T}$.

In **Figure 10(g–h)** for the relationship between the dimensionless output power and compound parameters, the value of $\varepsilon_0^2 RP_{\text{eff}}/\sigma^2 d_0^2$ increases with $\varepsilon_0 RS/d_0 T$ firstly and then reaches a constant. At the same time, the value of $T^2 P_{\text{eff}}/\sigma^2 S^2 R$ decreases with $\varepsilon_0 RS/d_0 T$ after being a constant when $\varepsilon_0 RS/d_0 T$ is smaller than 0.1. In **Figure 10 (k–l)**, a peak value is observed for $\varepsilon_0 TP_{\text{eff}}/\sigma^2 d_0 S$, which implies the optimal parameter combination for $\varepsilon_0 RS/d_0 T$ or $\overline{T}$. Similar to output voltage, output power may also be enhanced by tuning single parameter. For example, the remaining area S, period T, and equivalent thickness d_0 fixed, the best combination of $\varepsilon_0 RS/d_0 T$and A/l can be obtained for optimizing the output power for TENG by tuning load resistance R [26].

According to **Figures 8** and **10**, we can conclude that the scaling laws can provide a more comprehensive and rational optimization strategy for both contact-separation mode and sliding-mode TENG based on multiparameter analysis. The results can help enhance the output performance of the device as either a smart sensor or an energy harvester and may render a guideline for designing TENG devices.

Acknowledgements

This work was supported by the National Key R&D Program of China under grant No. 2018YFB1600200 and National Natural Science Foundation of China

under grant Nos. 11472244, 11621062, and 11772295 and the Fundamental Research Funds for the Central Universities under grant No. 2019QNA4040.

Author details

He Zhang* and Liwei Quan
College of Civil Engineering and Architecture, Zhejiang University, Hangzhou, China

*Address all correspondence to: zjuzhanghe@zju.edu.cn

References

[1] Wang ZL. Triboelectric nanogenerators as new energy technology and self-powered sensors—Principles, problems and perspectives. Faraday Discussions. 2014;**176**:447-458

[2] Wang ZL. On Maxwell's displacement current for energy and sensors: The origin of nanogenerators. Materials Today. 2017;**20**:74-82

[3] Oregan B, Gratzel M. A low-cost, high-efficiency solar cell based on dye-sensitized colloidal TiO_2 films. Nature. 1991;**353**:737-740

[4] Brennan L, Renew PO. Biofuels from microalgae—A review of technologies for production, processing, and extractions of biofuels and co-products. Sustainable Energy Reviews. 2010;**14**: 557-577

[5] Mago PJ, Blunden LS, Bahaj AS. Performance analysis of different working fluids for use in organic Rankine cycles. Proceedings of the Institution of Mechanical Engineers, Part A: Journal of Power and Energy. 2007;**221**:255-264

[6] Li Z, Zuo L, Luhrs G, Lin L, Qin Y. Electromagnetic energy-harvesting shock absorbers: Design, modeling, and road tests. IEEE Transactions on Vehicular Technology. 2013;**62**(3): 1065-1074

[7] Zhang H, Shen MZ, Zhang YY, Chen YS, Lu CF. Identification of static loading conditions using piezoelectric sensor arrays. ASME Journal of Applied Mechanics. 2018;**85**:011008-011005

[8] Chen YS, Zhang H, Zhang ZC, Lu CF. Theoretical assessment on piezoelectric energy harvesting in smart self-powered asphalt pavements. Journal of Vibration Engineering & Technologies. 2018;**6**(1):1-10

[9] Chen YS, Zhang H, Zhang YY, Li CH, Yang Q, Zheng HY, et al. Mechanical energy harvesting from road pavements under vehicular load using embedded piezoelectric elements. Journal of Applied Mechanics-Transactions of the ASME. 2016;**83**(8)

[10] Lu CF, Zhang YY, Zhang H, Zhang ZC, Shen MZ, Chen YS. Generalized optimization method for energy conversion and storage efficiency of nanoscale flexible piezoelectric energy harvesters. Energy Conversion and Management. 2018;**182**:34-40

[11] Zhang H, Ye GR, Zhang ZC. Acoustic radiation of a cylindrical piezoelectric power transformer. ASME Journal of Applied Mechanics. 2013;**80** (6) 061019(1-6)

[12] Yang Y, Zhang H, Lin ZH, Zhou YS, Jing Q, Su Y, et al. Human skin based triboelectric nanogenerators for harvesting biomechanical energy and as self-powered active tactile sensor system. ACS Nano. 2013;**7**(10): 9213-9222

[13] Ya Y, Hulin Z, Qingshen J, Yusheng Z, Xiaonan W, Zhonglin W. ACS Nano. 2013;**7**(8):7342-7351

[14] Changbao H, Chi Z, Xiaohui L, Limin Z, Tao Z, Weiguo H, et al. Self-powered velocity and trajectory tracking sensor array made of planar triboelectric nanogenerator pixels. Nano Energy. 2014;**9**:325-333

[15] Zhang H, Zhang JW, Hu ZW, Quan LW, Shi L, Chen JK, et al. Waist-wearable wireless respiration sensor based on triboelectric effect. Nano Energy. 2016;**59**:75-83

[16] Chen JK, Guo HW, Ding P, Pan RZ, Wang WB, Xuan WP, et al. Nano Energy. 2016;**30**:235-241

[17] Niu S, Liu Y, Wang S, Lin L, Zhou YS, Hu Y, et al. Theory of sliding-mode triboelectric nanogenerators. Advanced Materials. 2013;**25**(43):6184-6193

[18] Niu SM, Wang SH, Lin L, Liu Y, Zhou SY, Hu YF, et al. Theoretical study of contact-mode triboelectric nanogenerators as an effective power source. Energy & Environmental Science. 2013;**6**:3576

[19] Simiao N, Sihong W, Ying L, Shengyu Z, Long L, Youfan H, et al. A theoretical study of grating structured triboelectric nanogenerators. Energy & Environmental Science. 2014;**7**:2339

[20] Simiao N, Ying L, Sihong W, Long L, Yusheng Z, Youfan H, et al. Theoretical investigation and structural optimization of single-electrode triboelectric nanogenerators. Advanced Functional Materials. 2014;**24**: 3332-3340

[21] Simiao N, Yin L, Xiangyu C, Sihong W, Yusheng Z, Long L, et al. Theory of freestanding triboelectric-layer-based nanogenerators. Nano Energy. 2015;**12**: 760-774

[22] Yunlong Z, Simiao N, Jie W, Zhen W, Wei T, Zhonglin W. Standards and figure-of-merits for quantifying the performance of triboelectric nanogenerators. Nature Communications. 2015;**6**:8376

[23] Jiajia S, Tao J, Wei T, Xiangyu C, Liang X, Zhonglin W. Structural figure-of-merits of triboelectric nanogenerators at powering loads. Nano Energy. 2018;**51**:688-697

[24] Peng J, Kang SD, Snyder GJ. Optimization principles and the figure of merit for triboelectric generators. Science Advances. 2017;**3**:eaap 857615

[25] Zhang H, Quan LW, Chen JK, Xu CK, Zhang CH, Dong SR, et al. A general optimization approach for contact-separation triboelectric nanogenerator. Nano Energy. 2019;**56**:700-707

[26] Zhang H, Zhang CH, Zhang JW, Quan LW, Huang HY, Jiang JQ, et al. A theoretical approach for optimizing sliding-mode triboelectric nanogenerator based on multi-parameter analysis. Nano Energy. 2019. DOI: 10.1016/j.nanoen.2019.04.057